A Journal of the Gesellschaft Deutscher Chemiker

Angewandte International Edition GDCh Chemie

www.angewandte.org

Accepted Article

Title: The Microscopic Diamond Anvil Cell: Stabilization of Superhard, Superconducting Carbon Allotropes at Ambient Pressure

Authors: Xiaoyu Wang, Davide M Proserpio, Corey Oses, Cormac Toher, Stefano Curtarolo, and Eva Zurek

To be cited as: *Angew. Chem. Int. Ed.* **2022**, e202205129

Link to VoR: https://doi.org/10.1002/anie.202205129

WILEY-VCH

10.1002/anie.202205129

WILEY-VCH

COMMUNICATION

The Microscopic Diamond Anvil Cell: Stabilization of Superhard, Superconducting Carbon Allotropes at Ambient Pressure

Xiaoyu Wang,[a] Davide M Proserpio,[b] Corey Oses,[c,d] Cormac Toher,[d,e,f] Stefano Curtarolo,[c,d] and Eva Zurek*[a]

[a] X. Wang, Prof. E. Zurek
Department of Chemistry
State University of New York at Buffalo
Buffalo, NY 14260-3000, USA
E-mail: ezurek@buffalo.edu
[b] Prof. D. M. Proserpio
Dipartimento di Chimica
Universita' degli Studi di Milano
Via Golgi, 19-20133, Milano, Italy
[c] C. Oses, Prof. S. Curtarolo
Department of Mechanical Engineering and Materials Science
Duke University
Durham, NC 27708, USA
[d] C. Oses, Prof. C. Toher, Prof. S. Curtarolo
Center for Autonomous Materials Design
Duke University
Durham, NC 27708, USA
[e] Prof. C. Toher
Department of Materials Science and Engineering
University of Texas at Dallas
Richardson, TX 75080, USA
[f] Prof. C. Toher
Department of Chemistry and Biochemistry
University of Texas at Dallas, Richardson
TX 75080, USA

Supporting information for this article is given via a link at the end of the document.

Abstract: A metallic, covalently bonded carbon allotrope is predicted via first principles calculations. It is composed of an sp^3 carbon framework that acts as a diamond anvil cell by constraining the distance between parallel cis-polyacetylene chains. The distance between these sp^2 carbon atoms renders the phase metallic, and yields two well-nested nearly parallel bands that cross the Fermi level. Calculations show this phase is a conventional superconductor, with the motions of the sp^2 carbons being key contributors to the electron phonon coupling. The sp^3 carbon atoms impart superior mechanical properties, with a predicted Vickers hardness of 48 GPa. This phase, metastable at ambient conditions, could be made by on-surface polymerization of graphene nanoribbons, followed by pressurization of the resulting 2D sheets. A family of multifunctional materials with tunable superconducting and mechanical properties could be derived from this phase by varying the sp^2 versus sp^3 carbon content, and by doping.

Metallic, covalently-bonded materials are candidates for conventional, or phonon-mediated, superconductivity.[1] Vibrations associated with the metallic covalent bonds, such as the B-B σ bonds in MgB_2,[2] the C-C sp^3 bonds in boron doped diamond,[3] and the weak multi-centered H-H bonds in the hydrogenic clathrate cages of compressed superhydrides[4] are characterized by a large electron phonon coupling (EPC). The light mass of the constituent elements and the large density of states (DOS) at the Fermi level (E_F) is key to achieving a high superconducting critical temperature, T_c. One way metallic covalent materials can be made is via the formation of unusual bonding environments induced by the high pressures present within diamond anvil cells. Carbon is particularly attractive since its strong bonds result in large kinetic barriers, important for quenching metastable materials to atmospheric pressures, and enhanced mechanical properties such as high density, superior hardness and large bulk modulus. Herein, density functional theory (DFT) calculations are performed to propose a form of carbon that is superconducting and superhard, and could be synthesized under mild pressures. Because it is characterized by an sp^3 framework that behaves as a microscopic diamond anvil cell by constraining the distance between sp^2 carbons, key for its metallicity, we call it DAC-carbon. Modifications of this structure could lead to a family of superconducting, superhard, multifunctional materials with tunable properties.

Previously, we predicted low-energy superhard carbon allotropes using a multi-objective evolutionary algorithm that employed both the DFT energy, and Vickers hardness ($H_{v,Teter}$) estimated using shear moduli obtained via a machine learning (ML) model trained on the AFLOW database.[5] Forty-three novel superhard phases were found, and the topological properties of their carbon frameworks were analyzed. However, their electronic structures, bonding peculiarities, and propensity for superconductivity were not discussed.

Though most of the novel carbon allotropes were insulators with large gaps between the conduction and valence band, some were semiconductors, and two were metallic. DAC-carbon,

10.1002/anie.202205129

referred to as *Cmmm*-12b in Ref 5 is one of these. Its primitive cell can be constructed by inserting sp^2 carbon atoms in an all-cis-polyacetylene chain into the sp^3 framework of the quasi-lonsdaleite structure R_2L_2,[6] commonly referred to as Z-carbon, and listed in the SACADA database[7] with the topology **sie** (Figure 1). At zero pressure DAC-carbon was 230 meV/atom (5.37 kcal/mol) less stable than diamond (within the PBE functional), and its enthalpy fell below that of graphite above 40 GPa. Phonon calculations confirmed this phase was dynamically stable from 0-5 GPa at 0 K, and molecular dynamics (MD) simulations at 100, 200, 300 and 400 K on the 20 and 40 GPa ground state geometries illustrated they were kinetically stable. Moreover, our MD simulations on the zero pressure geometry showed that the sp^2 carbon atoms from adjacent polyacetylene layers only begin to interact at 1600 K, suggesting the kinetic barriers to decomposition are large. Using the ML (DFT) calculated shear modulus we found $H_{v,Teter}$ = 45 (48) GPa, as compared to 72 GPa for R_2L_2.[5] Insertion of the sp^2 atoms into R_2L_2 dramatically decreases its hardness, however thanks to its sp^3 framework DAC-carbon still falls above the superhard threshold.

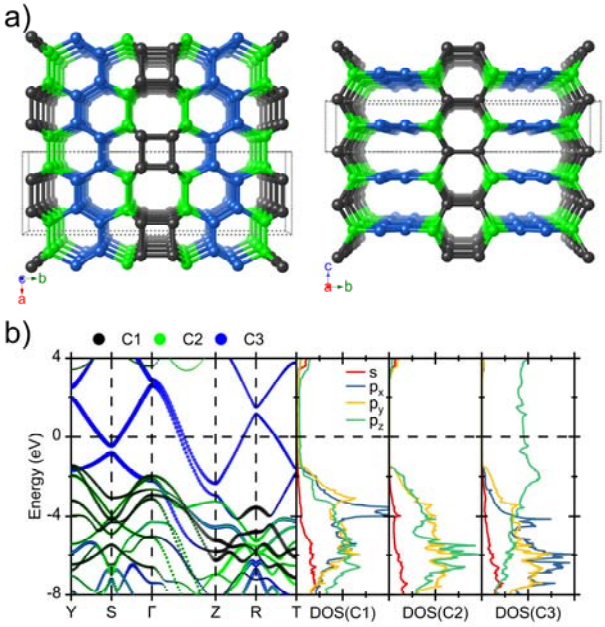

Figure 1. (a) Optimized structure of DAC-carbon with top view and side view. Its standard primitive cell contains 12 carbon atoms (8 sp^3 and 4 sp^2) and possesses the *Cmmm* spacegroup. Black balls are sp^3 carbon that are bonded only to other sp^3 carbons, green balls are sp^3 carbons bonded to both sp^3 and sp^2 carbons, and blue balls are sp^2 carbons; dashed lines denote the conventional cell. (b) Band structure along the Y (0.5,0.5,0) → S(0,0.5,0) → Γ(0,0,0) → Z(0,0,0.5) → R(0,0.5,0.5) → T(0.5,0.5,0.5) high symmetry lines, and orbital projected density of states (DOS, in states eV^{-1} $Å^{-3}$) for DAC-carbon. The thickness of the lines in the band structure denotes the contribution from the listed atom types.

As described fully in the Supplementary Information, a potential pathway for the realization of DAC-carbon would begin from 6-armchair graphene nanoribbons (6-AGNRs), which can nowadays be made with ease.[8] Analogous to the methods used to synthesize a biphenylene network with 4, 6 and 8-membered rings,[9] on-surface polymerization of the 6-AGNRs could be used to make a 2D precursor network, which was computed to be ~110 meV/atom more stable than the synthesized biphenylene network. This network is among one of many proposed by Li, He and co-workers in a high-throughput study of 2D carbon allotropes, where its properties were reported.[10] Finally, DAC-carbon would be synthesized by layering these sheets on top of each other followed by compression to ~20 GPa. Thus, DAC-carbon could potentially be synthesized under pressure, similar to the carbon phases observed upon cold compression of graphite,[11] or made using shock compression.[12]

The sp^2 chains in DAC-carbon propagate along the *a*-axis and are stacked along the *c*-axis. Their interlayer distance of 2.57 Å, dictated by the rigid framework of the sp^3 carbons, is considerably smaller than within the cis-polyacetylene crystal, with measured inter-chain distances of 4.4 Å.[13] This geometrical feature of DAC-carbon is reminiscent of the infinite polyene chains imagined by Hoffmann et al., whose interchain distance of 2.50 Å induced the metallicity in this hypothetical sp^2 carbon allotrope.[14] Hoffmann's work inspired the theoretical prediction of other 3D forms of carbon whose metallicity was induced by the steric confinement of the sp^2 carbon atoms.[15] Many of the predicted phases possessed a high hardness due to their large sp^3 ratio,[16–18] and the T_c of two that were not superhard was predicted to be 5 and 14 K,[19] but the mechanism of superconductivity was not analyzed.

The band structure and DOS plots of DAC-carbon (Figure 1(b)) clearly illustrates that their metallicity stems from the p_z orbitals of the sp^2 carbons. To explore this further we built a model where the sp^3 carbons of DAC-carbon, whose bond distances were nearly equal to those within diamond (1.57 Å vs. 1.55 Å), were removed from the cell and the dangling bonds were saturated by hydrogens. The resulting layered cis-polyacetylene chain possessed a repeating C_4H_4 unit where the C-C bonds measured 1.39 and 1.40 Å (c.f. 1.37 Å calculated for cis-polyacetylene), as in the relaxed DAC-carbon structure. Varying the interlayer distance, we computed the bandgap and estimated the internal pressure caused by the confinement from the negative of the change in energy versus volume, $P = -dE/dV$, as obtained numerically via the central difference method. Figure 2(a) illustrates that within the PBE-D3 (HSE-06) functionals the band gap closed when the interlayer distance was 4.15 (3.85) Å corresponding to a pressure of 0.19 (0.50) GPa. At the distance found in the optimized DAC-carbon lattice, the model system remained metallic and the internal pressure was calculated to be 15.9 GPa. Thus, the lattice of sp^3 carbons comprising DAC-carbon can be thought of as a microscopic diamond anvil that exerts pressure on the cis-polyacetylene chain, thereby inducing metallicity.

To better understand the origin of the insulator-to-metal transition, the PBE band structure of the cis-polyacetylene chain (Figure 2(b)) was analyzed. When the interaction between neighboring layers is small the highest occupied (lowest unoccupied) crystal orbital at the Zone center corresponds to the $1b_g$ ($2a_u$) symmetry linear combination of p_z orbitals that are π bonding (antibonding) along the shorter, and π anti-bonding (bonding) along the longer C-C distance, as illustrated schematically in the inset. At the Γ-point they are p_z σ anti-bonding with the next layer, whereas at the Z-point the p_z σ interaction is favorable. This interaction, insignificant at large distances due to the negligible orbital overlap, becomes increasingly important as the interlayer distance decreases. When the distance is the same as in DAC-carbon, the bands are pushed high above E_F at the Zone center, and they run down to the Z-point nearly parallel to

one another, as first proposed by Hoffmann for an all-sp^2 carbon analogue of the $ThSi_2$ structure.[14] Near E_F the band structure we calculate for the squeezed cis-polyacetylene chain model is in strikingly good agreement with the bands obtained for DAC-carbon (cf. Figure 2(b) and Figure 1(b)). Though the p_z σ bonding within DAC-carbon is weak (the integrated Crystal Orbital Hamilton Population for nearest neighbors is -0.06 eV/bond, cf. -9.5 eV/bond for the bonds in diamond), it is key for the metallicity of this phase.

This set of steep parallel bands separated by ~0.48 eV suggests a Fermi surface that is well nested. Could DAC-carbon be a covalently bonded conventional superconductor? To answer this question we calculated the phonon band structure, Eliashberg spectral function, the EPC parameter (λ = 0.37), and logarithmic average of the phonon frequencies (ω_{ln} = 670 K) for this phase. Within the Allen-Dynes modified McMillan equation, and using a renormalized Coulomb repulsion parameter characteristic of boron doped diamond, μ^* = 0.1, T_c was estimated to be 1.6 K. This value is strikingly close to the only known superconducting form of pure carbon, magic angle twisted bilayer graphene (T_c = 1.7 K), whose superconductivity is thought to be a result of strong electron correlations,[20] and somewhat lower than that of boron doped diamond (T_c = 4 K for a doping level of 2.5%).[21] The λ of DAC-carbon is similar to estimates for diamond doped with 1.85% boron,[22] even though its DOS at E_F is about a factor of five smaller.

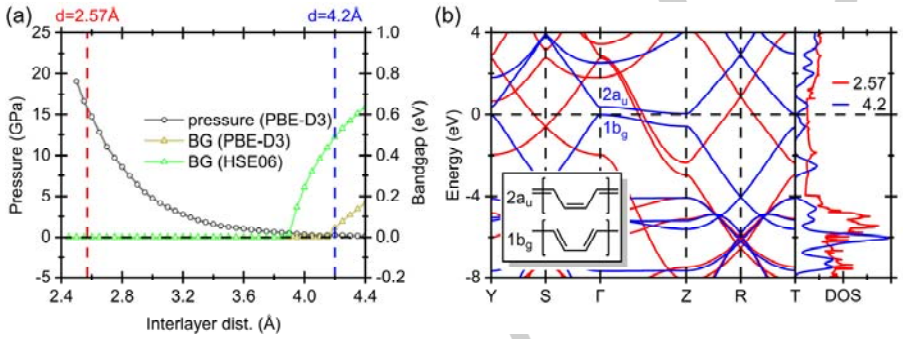

Figure 2. (a) Band gap of an ensemble of cis-polyacetylene chains for the given interlayer distances as calculated with the non-hybrid PBE-D3 (brown triangles) and hybrid HSE-06 (green triangles) functionals. The pressure at these interlayer distances as obtained with PBE-D3 is also provided (black circles). (b) Band structure as computed with the PBE functional for the cis-polyacetylene chain for interlayer distances of 4.20 Å (blue) and 2.57 Å (red). Since the interlayer spacing affects the c lattice constant, the length along the Γ−Z high-symmetry lines for the non-interacting chains has been scaled to match those whose distance is constrained to be the same as in DAC-carbon.

To analyze the nature of the pairing mechanism, we plotted the phonon band structure decorated by the EPC line-widths, whose thickness is proportional to the coupling strength (Figure 3(a)). A soft mode with a frequency of 156 cm^{-1} at the Z-point had the largest contribution, 26%, to the total λ. About 20% of λ was due to the four highest frequency bands, which are associated with the in-plane stretching modes of the sp^2 carbons. These bands are relatively flat, but soften significantly around the Z-point. Careful inspection of the Fermi surface plots showed that the two parallel bands crossing E_F along the Γ→ Z line are strongly nested, so that an electron travelling on one of the surfaces can absorb a phonon with wavevector **q** = (0,0,0.5) and be scattered on the other surface resulting in a large EPC ((Figure 3(b)). Visualization of the vibration associated with the 156 cm^{-1} mode showed that it corresponded to the rotation of a pair of sp^2 carbon atoms in the *cb* plane, with dimers in neighboring layers rotating in opposite directions, while the sp^3 carbons remain stationary. This motion modified the distance between carbon atoms comprising neighboring polyacetylene chains, and the p_z σ overlap between them.

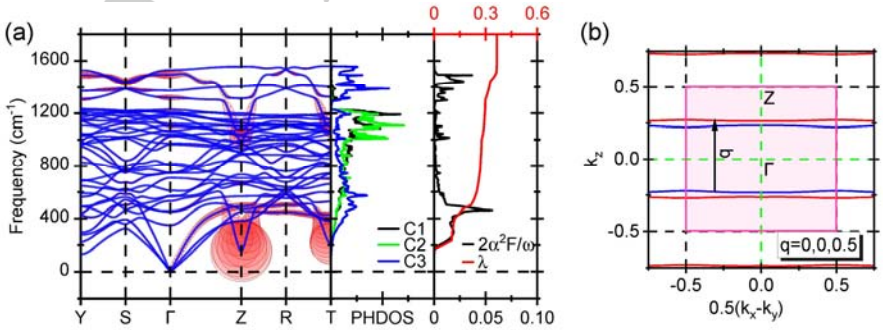

Figure 3. (a) Phonon band structure, atom projected phonon density of states (PHDOS), Eliashberg spectral function, in the form of $2\alpha^2F(\omega)/\omega$, and the electron phonon integral, $\lambda(\omega)$, for DAC-carbon. Red circles indicate the electron-phonon coupling constant, λ_{qv}, at mode *v* and wavevector **q**, and their radii is proportional to the strength. (b) Isocontour of eigenvalues for the two parallel bands $1b_g$ (blue) and $2a_u$ (red) at the Fermi level. The pink shaded region represents the first Brillouin zone. Black vector indicates the phonon vector **q** = (0,0,0.5) by which the two bands are nested.

Owing to the relatively heavy mass of carbon, the highest vibrational frequency in DAC-carbon is ~1600 cm^{-1}, and the ω_{ln} is relatively low. Because only the p_z orbitals of the sp^2 carbons contribute to the metallicity, the DOS at E_F is also low. Both of these T_c descriptors could be increased via boron doping, and ω_{ln} could be improved by inserting H_2 into the voids within the R_2L_2 lattice. Since the weak $p_z\sigma$ interaction, which is dependent on the interlayer distance, is key for the EPC, the T_c is likely pressure dependent. Indeed, our calculations show T_c increases to 8.3 K at 5 GPa. The R_2L_2 strips could be thickened thereby hardening the allotrope, but widening the sp^2 chains would soften the material and increase the number of states participating in the EPC mechanism. Finally, different sp^3 frameworks that comprise the microscopic diamond anvil can be chosen. We dream some of these multifunctional allotropes, where the carbon framework acts as a diamond anvil cell, will one day be experimentally realized.

Acknowledgements

E.Z. and X.W. acknowledge the NSF (DMR-2119065), E.Z., C.T., C.O., and S.C. acknowledge the DOD-ONR (N00014-16-1-2583), and C.T., C.O., and S.C. acknowledge the DOD-ONR MURI program (N00014-15-1-2863) for financial support. This work was performed in part at the University at Buffalo's Center for Computational Research (http://hdl.handle.net/10477/79221).

Keywords: carbon allotropes • density functional calculations • electronic structure • superconductors • superhard materials

[1] X. Blase, E. Bustarret, C. Chapelier, T. Klein, C. Marcenat, *Nat. Mater.* **2009**, *8*, 375–382.
[2] J. Kortus, I. I. Mazin, K. D. Belashchenko, V. P. Antropov, L. L. Boyer, *Phys. Rev. Lett.* **2001**, *86*, 4656.
[3] L. Boeri, J. Kortus, O. K. Andersen, *Phys. Rev. Lett.* **2004**, *93*, 237002.
[4] E. Zurek, T. Bi, *J. Chem. Phys.* **2019**, *150*, 050901.
[5] P. Avery, X. Wang, C. Oses, E. Gossett, D. M. Proserpio, C. Toher, S. Curtarolo, E. Zurek, *npj Comp. Mater.* **2019**, *5*, 89.
[6] R. Baughman, A. Liu, C. Cui, P. *Schields, Synth. Met.* **1997**, *86*, 2371-2374.
[7] R. Hoffmann, A. A. Kabanov, A. A. Golov, D. M. Proserpio, *Angew Chem. Int. Edit.* **2016**, *55*, 10962-10976.
[8] N. Merino-Díez, J. Lobo-Checa, P. Nita, A. Garcia-Lekue, A. Basagni, G. Vasseur, F. Tiso, F. Sedona, P. K. Das, J. Fujii et al., *J. Phys. Chem. Lett.* **2018**, *9*, 2510–2517.
[9] Q. Fan, L. Yan, M. W. Tripp, O. Krejčí, S. Dimosthenous, S. R. Kachel, M. Chen, A. S. Foster, U. Koert, P. Liljeroth et al., *Science* **2021**, *372*, 852–856.
[10] X. Shi, S. Li, J. Li, T. Ouyang, C. Zhang, C. Tang, C. He, J. Zhong, *J. Phys. Chem. Lett.* **2021**, *12*, 11511-11519.
[11] W. L. Mao, H.-k. Mao, P. J. Eng, T. P. Trainor, M. Newville, C.-c. Kao, D. L. Heinz, J. Shu, Y. Meng, R. J. Hemley, *Science* **2003**, *302*, 425-427.
[12] C. He, C. Zhang, H. Xiao, L. Meng, J. Zhong, *Carbon* **2017**, *112*, 91–96.
[13] R. Baughman, S. Hsu, G. Pez, A. Signorelli, *J. Chem. Phys.* **1978**, *68*, 5405-5409.
[14] R. Hoffmann, T. Hughbanks, M. Kertesz, P. H. Bird, *J. Am. Chem. Soc.* **1983**, 105, 4831-4832.
[15] M. J. Bucknum, R. Hoffmann, *J. Am. Chem. Soc.* **1994**, *116*, 11456-11464.
[16] X. Wu, X. Shi, M. Yao, S. Liu, X. Yang, L. Zhu, T. Cui, B. Liu, *Carbon* **2017**, *123*, 311-317.
[17] L. Liu, M. Hu, Z. Zhao, Y. Pan, H. Dong, *Carbon* **2020**, *158*, 546-552.
[18] Y. Liu, X. Jiang, J. Fu, J. Zhao, *Carbon* **2018**, *126*, 601-610.
[19] M. Hu, X. Dong, B. Yang, B. Xu, D. Yu, J. He, *Phys. Chem. Chem. Phys.* **2015**, *17*, 13028-13033.
[20] Y. Cao, V. Fatemi, S. Fang, K. Watanabe, T. Taniguchi, E. Kaxiras, P. Jarillo-Herrero, *Nature* **2018**, *556*, 43-50.
[21] E. Ekimov, V. Sidorov, E. Bauer, N. Mel'Nik, N. Curro, J. Thompson, S. Stishov, *Nature* **2004**, *428*, 542-545.
[22] X. Blase, C. Adessi, D. Connétable, *Phys. Rev. Lett.* **2004**, *93*, 237004.
[23] V. A. Blatov, O. A. Blatova, F. Daeyaert, M. W. Deem, *RSC Adv.* **2020**, *10*, 17760-17767.

10.1002/anie.202205129

WILEY-VCH

COMMUNICATION

Entry for the Table of Contents

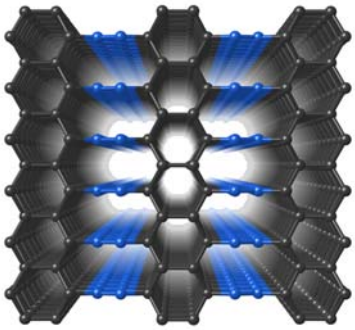

DAC-Carbon: The superhard sp^3 framework serves as a microscopic diamond anvil cell, in which the sp^2 chains are compressed to establish the metallicity and superconductivity.

Supporting Information for: "The Microscopic Diamond Anvil Cell: Stabilization of Superhard, Superconducting Carbon Allotropes at Ambient Pressure"

Xiaoyu Wang, Davide M Proserpio, Corey Oses,
Cormac Toher, Stefano Curtarolo, and Eva Zurek*

June 5, 2022

Contents

S1 Computational Methods

Geometry optimizations, molecular dynamics (MD), and electronic structure calculations were performed using density functional theory with the PBE functional[1] as implemented in the Vienna *Ab initio* Simulation Package (VASP).[2] The plane wave basis set was set to a 600 eV cutoff to treat the valence electrons (H $1s^1$, C $2s^2 2p^4$), while the core electrons were treated with the projector augmented wave method.[3] The reciprocal space was sampled using a Γ-centered Monkhorst-Pack mesh[4] where the number of divisions along each reciprocal lattice vector was chosen such that the product of this number with the real-space lattice constant was 70 Å for the density of states calculations, and 50 Å otherwise in the static calculations. The MD simulations were carried out on a $2 \times 1 \times 3$ supercell of the conventional cell that contained 144 carbon atoms, and only the Γ point was sampled.

The pressure exerted by the microscopic diamond anvil was calculated using Grimme's D3 dispersion correction (PBE-D3),[5] and band gaps were obtained using the PBE-D3 and HSE06[6] functionals. The crystal orbital Hamilton populations (COHPs)[7] and the negative of the COHPs integrated to the Fermi level (-iCOHPs) were calculated using the LOBSTER package (v4.0.0),[8] and the results used to analyze the bonding. The Vickers hardness of select structures at ambient pressure was calculated via the Teter equation ($H_{\text{v,Teter}} = 0.151G$)[9] using the shear moduli, G, obtained from the machine learning (ML) model trained on the AFLOW database.[10,11]

Dynamic stability was determined via phonon calculations performed using the finite difference scheme as implemented in the Phonopy software package.[12] The finite-temperature kinetic stability of DAC-carbon was probed via MD simulations performed using a canonical (NVT) ensemble coupled with the Nosé-Hoover thermostat.[13,14] Simulations were carried out at select temperatures and volumes (corresponding to 0 K pressures noted below) for a total of 2.5 ps using a 0.5 fs time-step. In all of the runs conducted, equilibration of the energy and temperature was observed by $\sim$0.2 ps.

The electron-phonon coupling (EPC) calculations for DAC-carbon were carried out with the PBE functional as implemented in the Quantum Espresso (QE) package version 5.2.[15] The core and inner shell electrons were simulated with the PSLibrary[16] projector augmented wave pseudopotential. An 80 Ry energy cutoff was employed to reach a convergence of 1 meV/atom for the cohesive energy. The electronic eigenvalues were calculated using a large $36 \times 36 \times 48$ k-mesh, and the phonon and EPC matrix elements were calculated using a small $12 \times 12 \times 16$ k-mesh and interpolated to the large mesh to calculate the phonon linewidths. The phonons were calculated using a $6 \times 6 \times 8$ q-mesh.

Convergence tests were performed to find the optimal k-mesh for the EPC calculations. The EPC matrix elements were calculated over a small grid, k_1, then interpolated to a large grid, k_2, on which the electronic eigenstates at the Fermi level were counted. The $(0, 0, -0.5)$ q-point was chosen for the convergence tests. First we tested the k_1 mesh, while the k_2 mesh was fixed to $6 \times 6 \times 8$. The electron phonon coupling constant, $\lambda_{\mathbf{q}j}$, was calculated with a series of k_1 meshes, and the results are displayed in Figure S1a and S1b for the 1$^{\text{st}}$ and 26$^{\text{th}}$ mode, respectively. Our results showed that $\lambda_{\mathbf{q}j}$ was converged using a Gaussian broadening with a width of $\sigma = 0.015$ Ry and a k_1 mesh of $36 \times 36 \times 48$. Similar tests for the k_2 mesh were performed with a fixed k_1 mesh of $36 \times 36 \times 48$, showing that $\lambda_{\mathbf{q}j}$ converges with a k_2 mesh of $12 \times 12 \times 16$ (Figure S1c and S1d). The superconducting critical temperature, T_c, was estimated using the Allen-Dynes

modified McMillan equation

$$T_{\rm c} = \frac{\omega_{\rm ln}}{1.2} \exp\left[-\frac{1.04(1+\lambda)}{\lambda - \mu^*(1+0.62\lambda)}\right], \tag{1}$$

with a Coulomb renormalization parameter, μ^* =0.1.[17] The EPC constant, λ, and logarithmic average of the phonon frequencies, $\omega_{\rm ln}$, were obtained from the QE calculations.

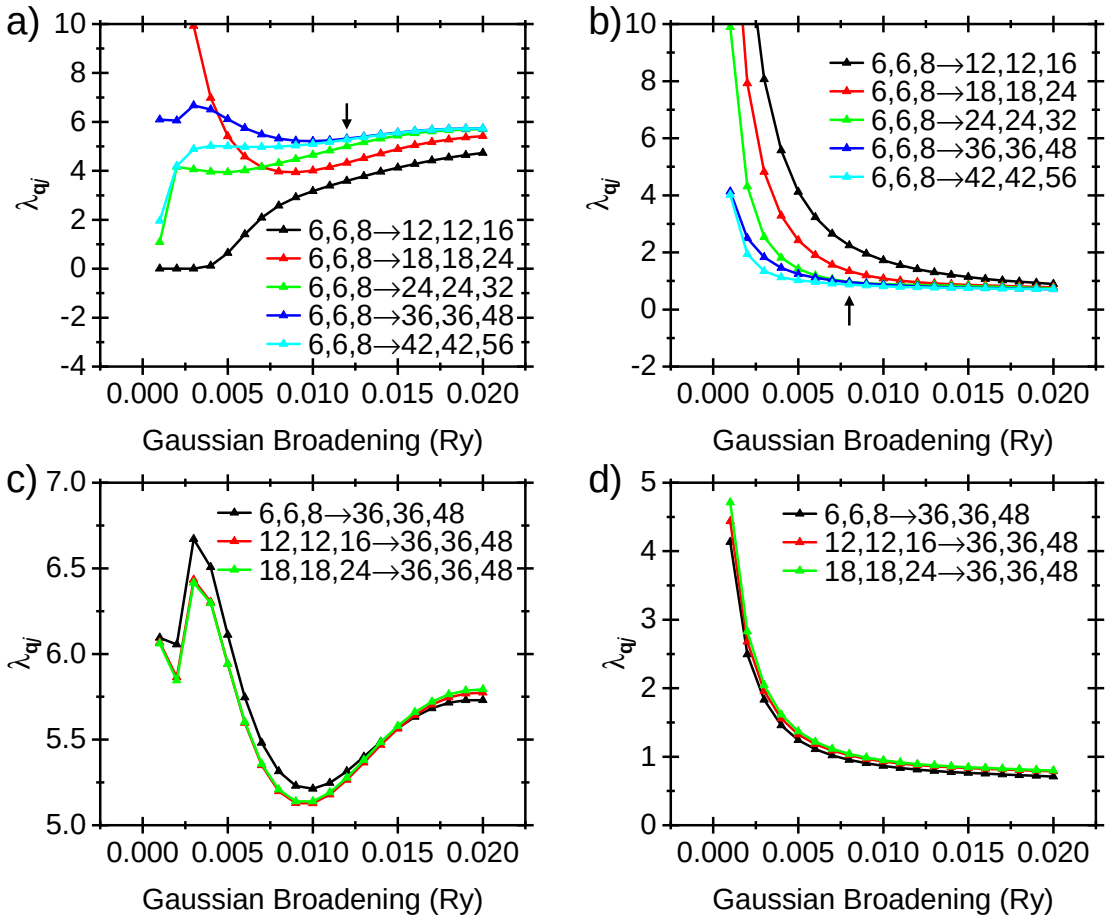

Figure S1: Electron-phonon coupling constant, $\lambda_{\mathbf{q}j}$, versus Gaussian broadening width at $q = (0, 0, -0.5)$ for the (a) $1^{\rm st}$ and (b) $26^{\rm th}$ phonon mode with a fixed k_2 mesh; (c) the $1^{\rm st}$ and (d) $26^{\rm th}$ phonon mode with a fixed k_1 mesh. In (a) and (b) the black arrows show where the $\lambda_{\mathbf{q}j}$ are considered to be converged.

S2 Previously Predicted Metallic Carbons

In 1983 Hoffmann, Hughbanks, Kertesz and Bird proposed an all-sp^2 carbon structure in which infinite polyacetylene chains running in two dimensions are packed to form a carbon crystal.[18] This is the $ThSi_2$ structure that is assumed by many materials. In the carbon analogue the interlayer distance would be constrained to 2.494 Å if a C-C distance of 1.44 Å is assumed. This network, later-on called bct-4 carbon,[19] is metallic due to the p-p σ and potentially p-p π overlap. Several years later another all-sp^2 carbon network that is topologically related to diamond, H-6 carbon, was proposed,[20] followed by "glitter",[21] which contains layers of polycyclic benzene chains.

Since then a plethora of metallic carbon allotropes have been hypothesized, and they can be classified according to the metallization strategy. These include a) 3-coordinated (sp^2) carbon: K_4 (NO. 5 in the SACADA database with the topological name **srs**, same below);[22] b) Distorted 4-coordinated (sp^3) carbon: Tri-C_9 (31 **afw**),[23] K_6-carbon (12 **lcv**),[24] and h-C_{63};[25] c) Compression of graphene or carbon nanotubes: 3D-GNR,[26] carbon foams (113 **xci**, 251 3^5,4T6, and 320 3^9,4T1),[27] 3D(4,0)-II and 3D(6,0)-II (133 sqc6952 and 139 3,4T86);[28] d) Splicing of sp^2 units and sp^3 networks: H18-carbon (165 $3,4^2$T223),[29] C14-diamond,[30] (3,0)/(4,0) and (6,0) honeycomb structures (183 $3,4^2$T209 and 113 **xci**),[31] oC16 (210 $3,4^3$T72),[32] GT-8 and CT-12 (108 **clh** and 126 sqc3051),[33] O-carbons and T-carbons,[34] orth-10 and orth-10′,[35] superpentalene,[36] C10,[37] as well as Hex-C_{72}.[38]

In some cases the predicted phases are true metals with partially filled bands. In other cases, the calculated metallicity may be an artifact of the choice of the density functional in the electronic structure calculations. For example, oC36 was reported to be a metal based on LDA calculations.[39] However, we recalculated its band structure at 4 and 25 GPa (Figure S2) with the PBE functional. An indirect bandgap of 0.22 eV was obtained at 4 GPa, and the bandgap was just closed at 25 GPa. Hybrid functionals such as HSE06 are likely to yield an even larger gap. Therefore, it is unlikely the phase is superconducting at 4 and 25 GPa as reported in Ref.[39]

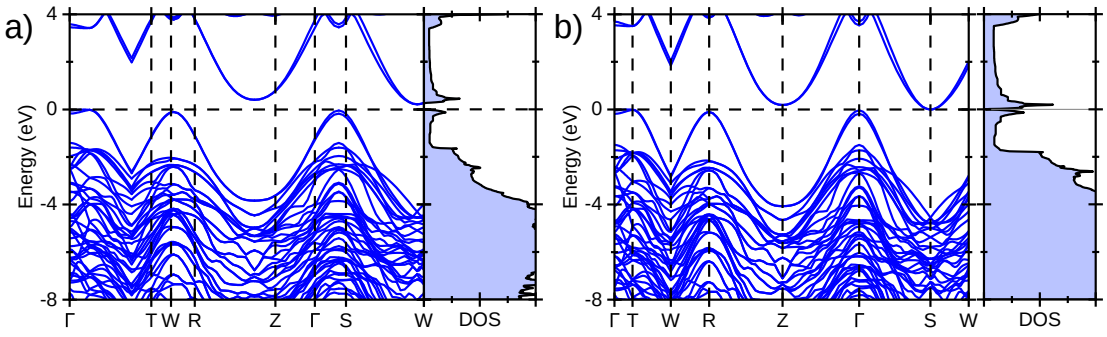

Figure S2: PBE bandstructure for oC36 at a) 4 GPa and b) 25 GPa.

We now comment on the potential superconductivity of some of the previously reported phases that have parallel bands crossing the Fermi level, also potentially suggestive of Fermi surface nesting. The all-sp^2 structure "glitter" has an interlayer distance of 2.60 Å at ambient pressure. We performed electron-phonon coupling calculations for glitter on a 16×16×8 k-mesh and a 8×8×4 q-mesh. These settings yielded a λ of 0.17 and a $\omega_{\ln}$ of 1038 K. Using the Allen-Dynes modified McMillan equation the T_c was estimated to be as small as 0 K for $\mu^* = 0.1$. At

40 GPa the glitter structure was on the edge of dynamic instability (with an interlayer distance of 2.50 Å), yielding $\lambda = 0.25$, $\omega_{\ln} = 804$ K, and $T_c = 0.03$ K.

The superconducting properties of these other phases have not been calculated yet: bct-4 carbon contains layered *trans*-polyacetylene chains and possesses nested parallel bands crossing the Fermi level,[19] suggesting it may be superconducting. Hex-C_{72}-I and -II[38] both contain a layered hexagonal sp^2 unit composed of 12 carbon atoms, while the interlayer distance is restricted by the hollowed sp^3 framework. The large primitive cell of both Hex-C_{72} phases contains multiple parallel bands crossing the Fermi level, and can be nested at various **q**-vectors. This suggests that both both Hex-C_{72}-I and -II possess relatively large EPC and exhibit superconductivity. GT-8[33] is made from the same sp^3 ribbon as DAC-carbon, while its sp^2 portion resembles glitter, and it has very well nested parallel bands at the Fermi level. Indeed, this phase was predicted to have a T_c of 5.2 K,[33] though it is not superhard. GT-16 is predicted to have a T_c of 14.0 K, and CT-12 also possesses parallel bands.[33] The calculations performed on GT-8/GT-16 further suggest that varying the sp^2/sp^3 ratios and topology of the sp^2 portions can be used to tune the superconducting and mechanical properties of these carbon allotropes.

S3 Electronic Structure of Mixed sp^2/sp^3 Carbon Phases

In Ref.[11] we employed a novel evolutionary algorithm that used DFT-energies and ML-shear moduli based estimates of the Vickers hardness to predict superhard carbon allotropes. Forty-three new superhard, low energy phases were found. In Fig. S3 we illustrate those that contained both sp^3 and sp^2 hybridized carbon atoms. The naming scheme used is the same as in Ref.[11]

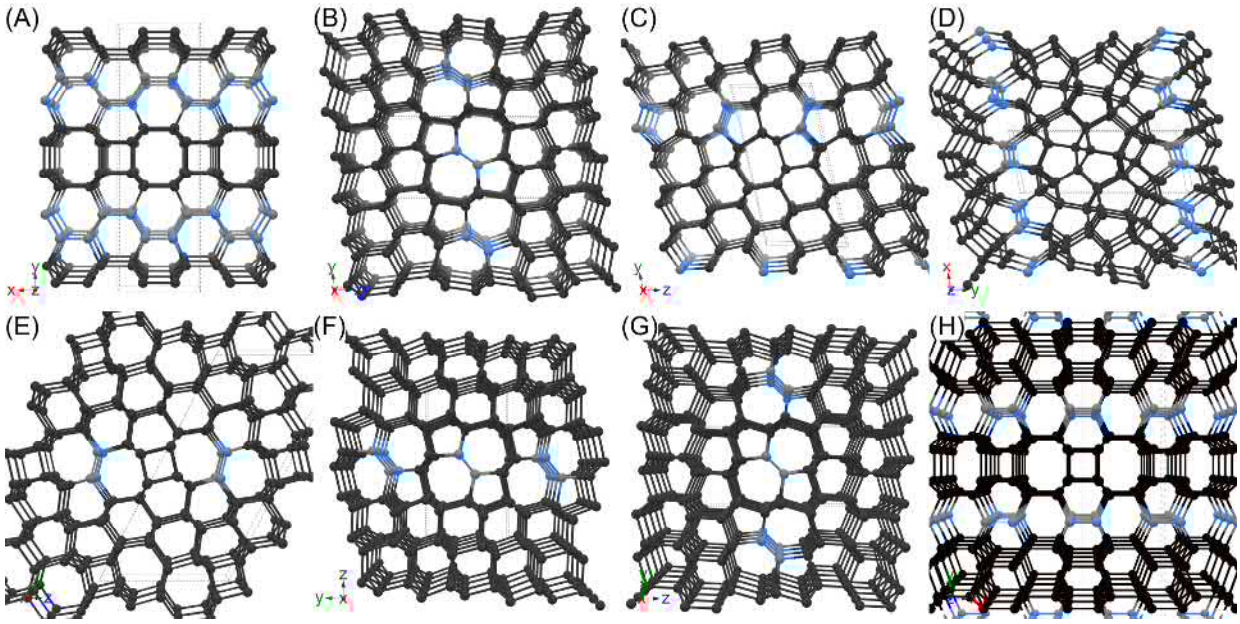

Figure S3: Optimized structure of: (a) $Cmmm$-12b (DAC-carbon), (b) $P\bar{1}$-16b, (c) $P1$-16a, (d) $P1$-16b, (e) $C2/m$-16b, (f) $P\bar{1}$-16c, (g) $P\bar{1}$-16e, and (h) $Cmmm$-20. The sp^2 atoms are illustrated in blue color, and the unit cell is shown with a faint dashed line.

structure	E_{ref}	$H^{\text{ML}}_{\text{v,Teter}}$	BG_{PBE}	BG_{HSE}	BG type
DAC-carbon	0.23	44.6	0	0	-
$Cmmm$-20	0.23	52.4	0	0	-
$C2/m$-16b	0.19	67.8	0.0	0.5	indirect
$P1$-16a	0.28	67.5	0.6	1.5	indirect
$P\bar{1}$-16e	0.26	71.5	0.9	1.9	indirect
$P\bar{1}$-16c	0.24	71.3	1.1	2.0	indirect
$P\bar{1}$-16b	0.26	72.4	1.2	2.2	indirect
$P1$-16b	0.28	45.3	2.1	3.1	direct

Table S1: Properties of carbon allotropes containing sp^3 and sp^2 carbons at 0 GPa (Figure S3). Energy relative to graphite (E_{ref} in eV/atom), Vickers hardness as estimated via Machine Learned Shear moduli and the Teter model ($H^{\text{ML}}_{\text{v,Teter}}$ in GPa), band gap (BG) as calculated with the PBE and HSE-06 functionals (eV), and band gap type.

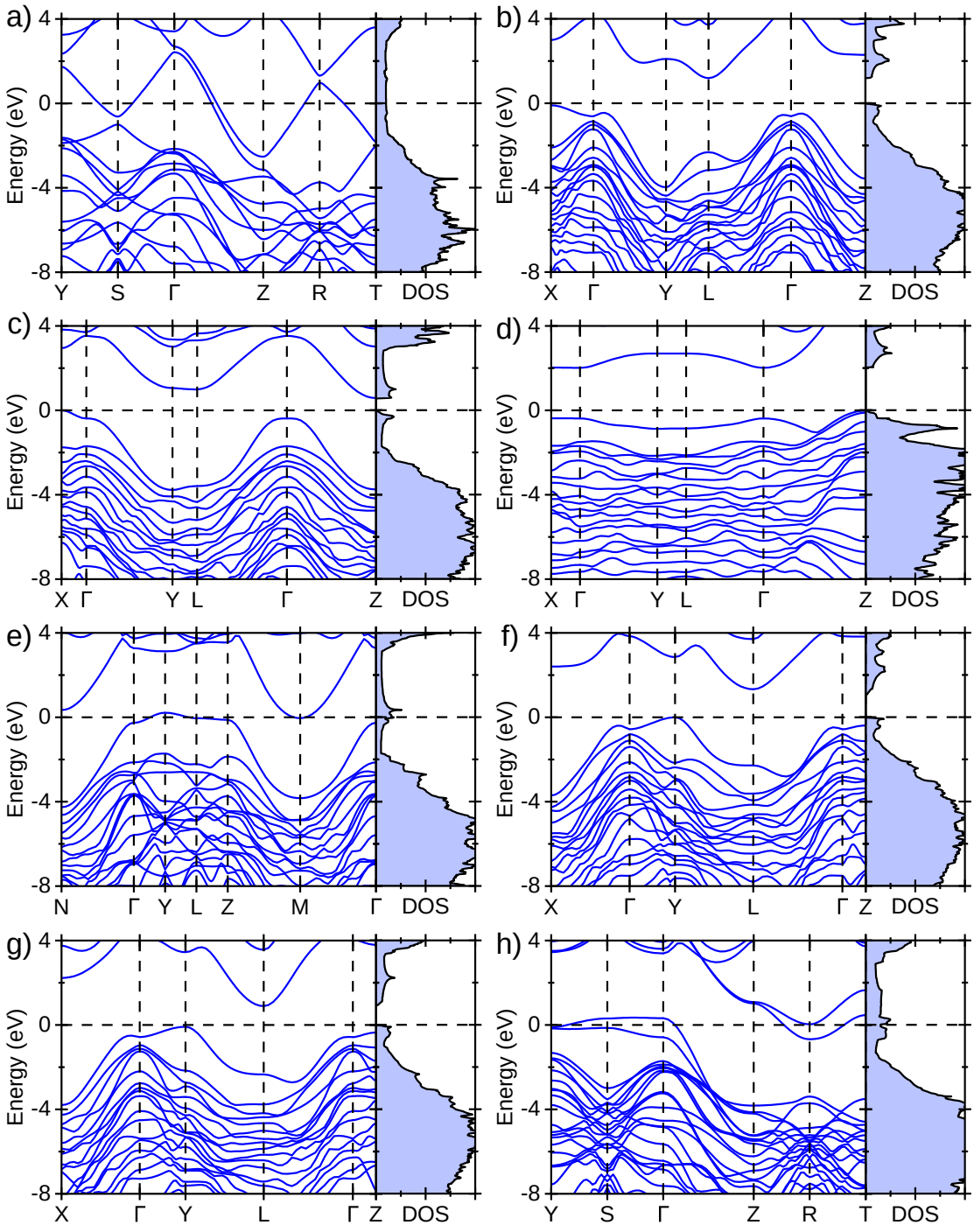

Figure S4: PBE band structure and density of states (DOS) for (a) DAC-carbon, (b) $P\bar{1}$-16b, (c) $P1$-16a, (d) $P1$-16b, (e) $C2/m$-16b, (f) $P\bar{1}$-16c, (g) $P\bar{1}$-16e, and (h) $Cmmm$-20.

S4 Properties of DAC-Carbon

S4.1 Electron Phonon Coupling under Pressure

At 0 K DAC-carbon was confirmed to be dynamically stable at 0 and 5 GPa. At 5 GPa the soft mode at the Z-point becomes almost imaginary (Figure S5a), which yields a large electron-phonon coupling constant of $\lambda = 0.67$, along with a $\omega_{\ln} = 269$ K, resulting in a T_c of 8.3 K. A comparison of $\frac{2\alpha^2F(\omega)}{\omega}$ between 0 and 5 GPa is shown in Figure S5b. The modes between 0-200 cm^{-1} greatly improved the EPC at 5 GPa, while the contribution from the high frequency modes are about the same.

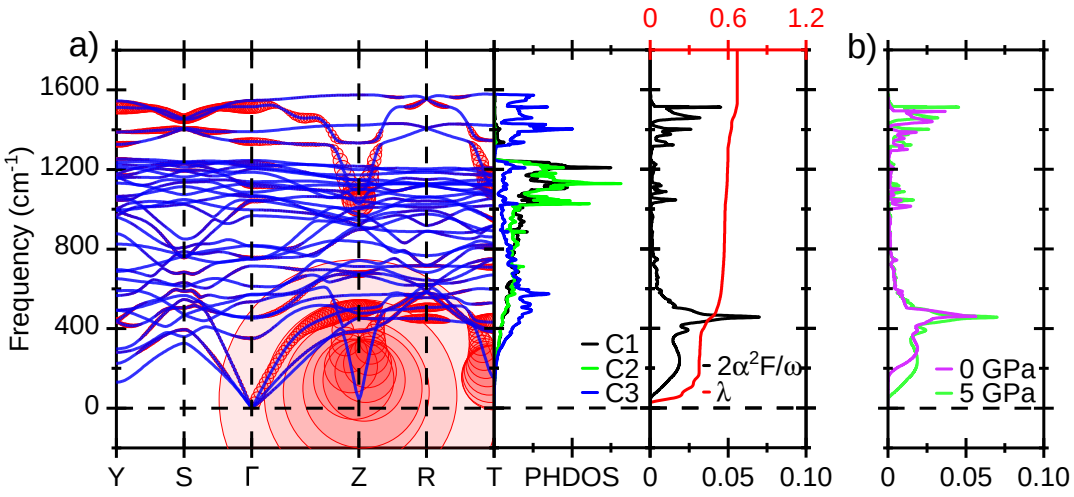

Figure S5: a) Phonon band structure, atom projected phonon density of states (PHDOS), Eliashberg spectral function, in the form of $\frac{2\alpha^2F(\omega)}{\omega}$, and the electron phonon integral, $\lambda(\omega)$, for DAC-carbon at 5 GPa. Red circles indicate the electron-phonon coupling constant, $\lambda_{\mathbf{q}\nu}$, at mode ν and wavevector $\mathbf{q}$, and their radii is proportional to the strength, using the same scale as in the main text Figure 3. b) A comparison of $\frac{2\alpha^2F(\omega)}{\omega}$ between 0 and 5 GPa.

S4.2 Fermi Surface Nesting

The eigenvalues were calculated on three different slices of k-space as shown in Figure S6a. The green slice cuts through the Γ (0, 0, 0) - Z (0, 0, 0.5) - T (0.5, 0.5, 0.5) plane, the pink slice cuts through Γ-Z and is perpendicular to Z-T, and the purple slice is parallel to the pink slice but crosses the T point (i.e. purple is pink shifted by **k** = (0.5, 0.5, 0.5)).

The nesting of the two parallel bands ($1b_g$ and $2a_u$) were analyzed on the above slices using the phonon vectors $\mathbf{q}_1$ = (0, 0, 0.5) and $\mathbf{q}_2$ = (0.5, 0.5, 0.5). On the green cut $1b_g$ (blue contours) and $2a_u$ (red contours) are poorly nested by both vectors (Figure S6b and c). However, on the pink cut $2a_u$ is perfectly nested with $1b_g$ by vector $\mathbf{q}_1$ as shown in Figure S6e. $\mathbf{q}_2$ is outside the pink slice, therefore we project the eigenvalues from the purple to the pink slice by shifting the purple by **-q**$_2$. The projected eigenvalues of the $1b_g$ band are displayed in Figure S6e with dashed

blue lines, and we found it largely nested with the $2a_u$ band, but the match is not as good as with $\mathbf{q}_1$. This explains the large electron-phonon coupling at the Z and T points in Figure 3a and S5a (because both phonon vectors result in good nesting at the Fermi level), and also explains why the EPC at the Z point is much larger than at T point (because the Z point has better nesting than T). The full Fermi surface is shown in Figure S6d.

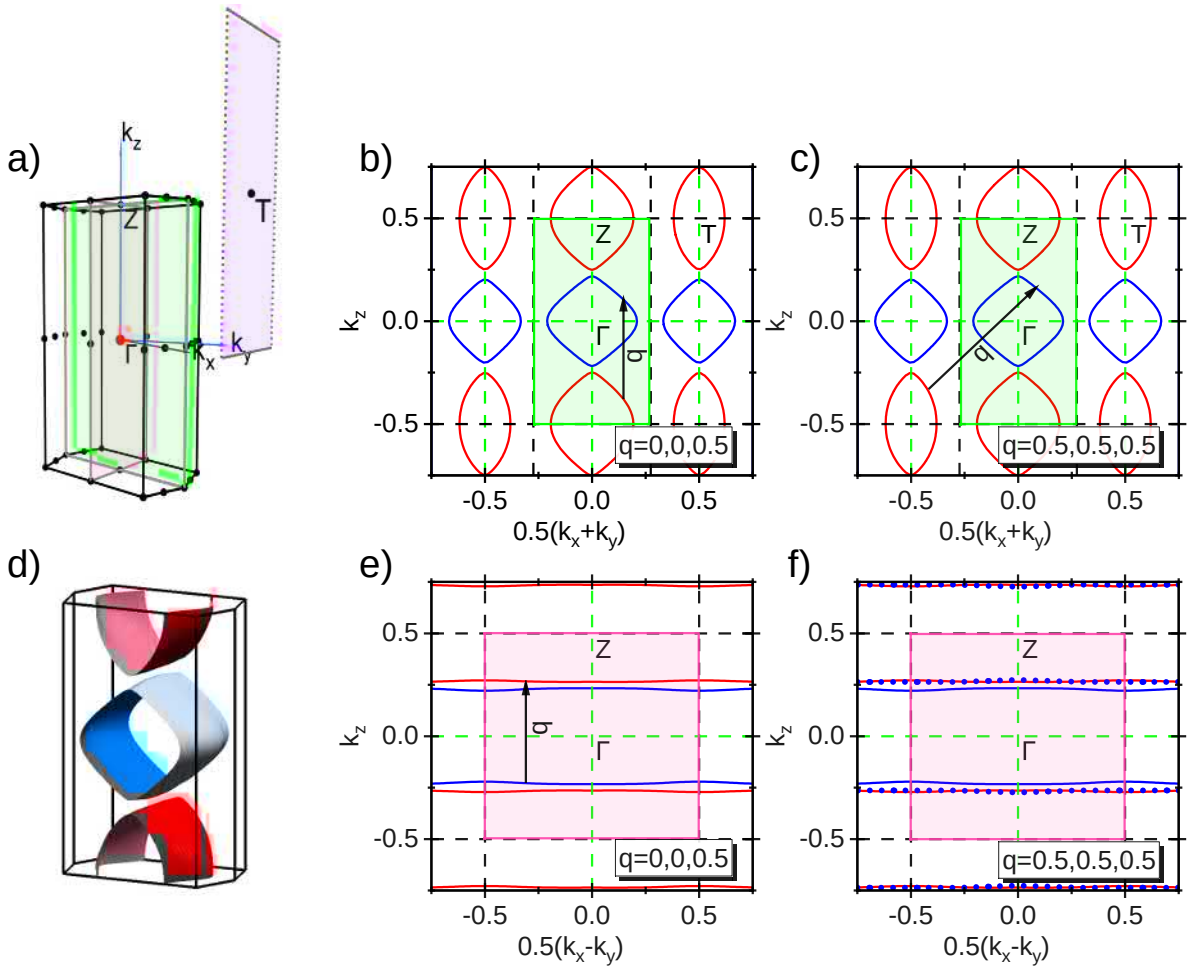

Figure S6: Two dimensional iso-energy contour for DAC-carbon at the Fermi level. a) The cutting slices used to displace the Fermi surface contours. The Fermi surface nesting on the green cut with phonon vectors b) (0, 0, 0.5) and c) (0.5, 0.5, 0.5). d) 3D Fermi surface in the first Brillouin zone. e) The Fermi surface nesting on the pink cut with phonon vector (0, 0, 0.5), and f) projections of the eigenvalues on the purple slice to the pink one by applying the phonon vector (-0.5, -0.5, -0.5)

S4.3 The Stacking Poly-acetylene Model

Changing the interlayer distance is a reversible process for which the differential statement of the first law of thermodynamics gives:

$$dU = TdS - PdV, \tag{2}$$

for T = 0 we have:

$$P = -\frac{dU}{dV} \approx -\frac{\Delta U}{\Delta V}. \tag{3}$$

To approximate the internal pressure the DFT energy was taken as the internal energy U, where the van der Waals interaction was treated via the DFT-D3 correction.[5] The central differential was applied to obtain the slope, i.e. $P_i = -(U_{i+1} - U_{i-1})/(V_{i+1} - V_{i-1})$ in which i is the i^{th} interlayer distance in Figure 2 in the main text.

In addition, the bandgaps were calculated with the PBE functional, revealing an indirect bandgap at large interlayer distances, where the conduction band minimum (CBM) was located at the Z point, and the valence band maximum (VBM) at the Γ point. The HSE06 bandgap was recalculated with a small set of *k*-points (Γ-centered 4^3).

Crystal orbital theory was employed to explain the metallicity. In the C_4H_4 model all electrons are paired except those in the four carbon p_z orbitals. These can be used to construct the four crystal orbitals shown in Figure S7, labelled using the naming convention from the C_{2h} point group. Considering the isolated C_4H_4 chain, the all-bonding $1a_u$ and all-anti-bonding $2b_g$ crystal orbitals are far from the Fermi level, while the two $1b_g$ and $2a_u$ frontier orbitals possess similar energies. $1b_g$/$2a_u$ is slightly more/less stable in our system due to the small difference between the two bond lengths (1.39 vs. 1.40 Å), which creates the small band gap, ΔE, between them.

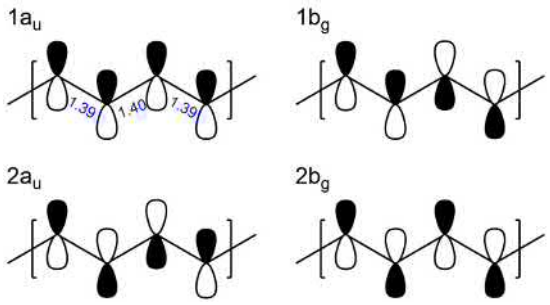

Figure S7: Crystal orbitals for the infinite C_4H_4 model. The unit cell is denoted by the brackets.

When the C_4H_4 chains are compressed together, the $p_z - p_z$ σ interaction perpendicular to the C-H plane starts to be established. At the Γ point the interaction is anti-bonding so the $1b_g$ and $2a_u$ bands increase in energy rising above the Fermi level, while at the Z-point it is bonding so the bottom of the band falls below the Fermi level. As a result, the two set of bands that "run down" from Γ-Z are responsible for the metallicity.

S4.4 Molecular Dynamics Simulations of DAC-carbon

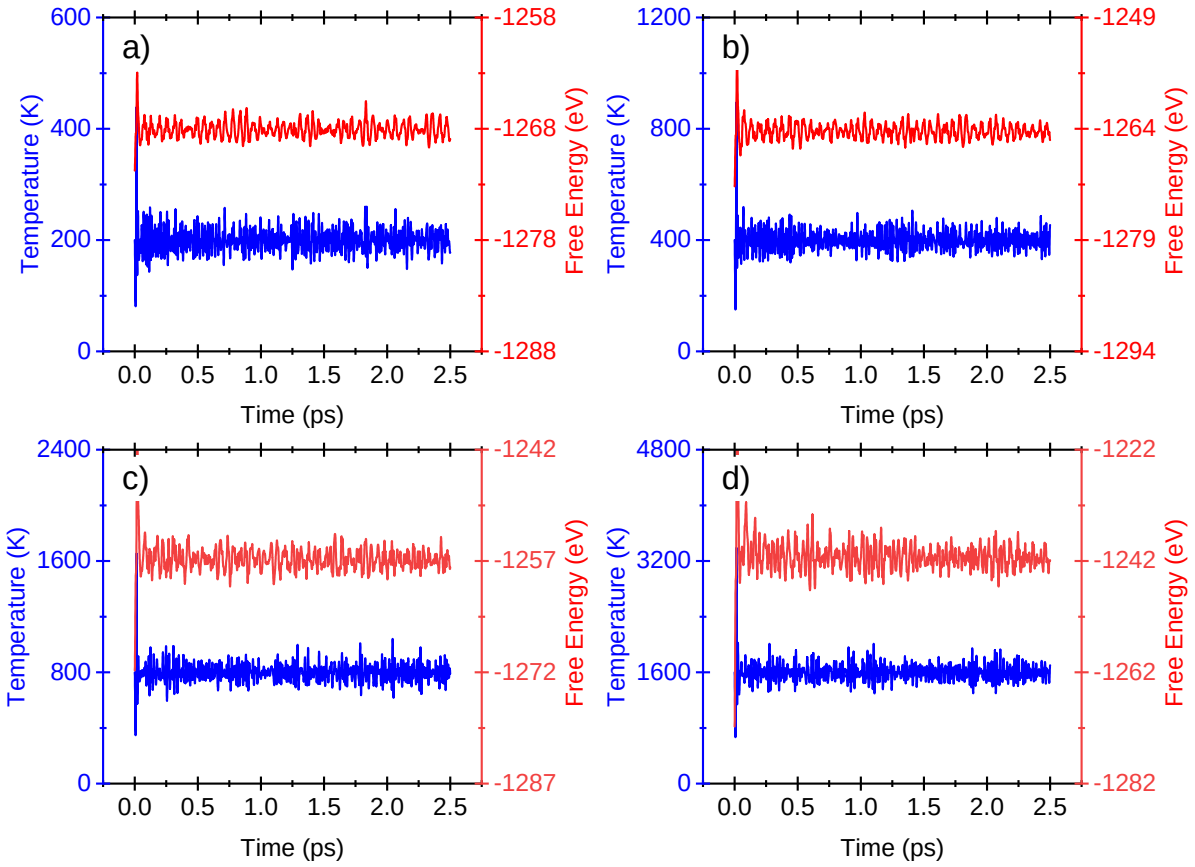

Figure S8: Temperature and energy profile for DAC-carbon at 0 GPa and: (a) 100 K, (b) 200 K, (c) 300 K, and (d) 400 K. All systems reached equilibrium within 0.2 ps.

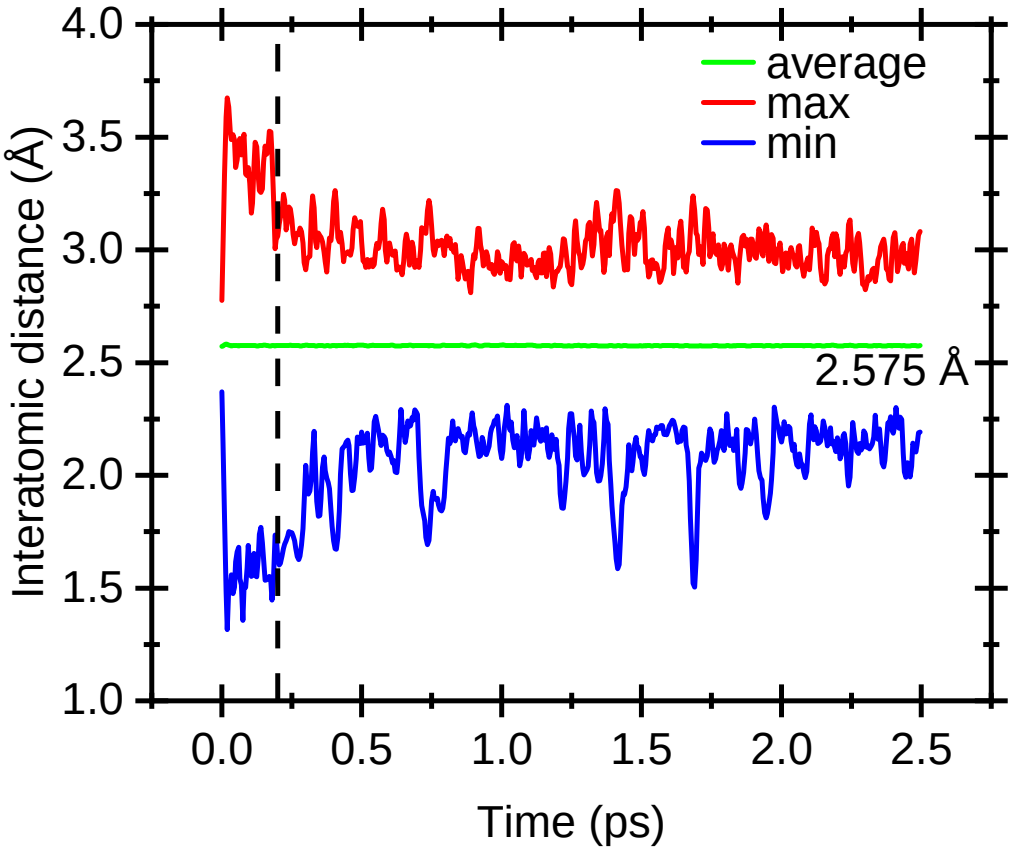

Figure S9: The minimum and maximum interatomic distance between pairs of carbon atoms comprising adjacent cis-polyacetylene chains in a molecular dynamics simulation carried out at 1600 K. The system is equilibrated by 0.2 ps (black dashed line). The average interatomic distance between nearest neighbor interlayer sp^2 atoms is given by the solid green line (2.575 Å, as compared to the 2.571 Å in the 0 K static structure).

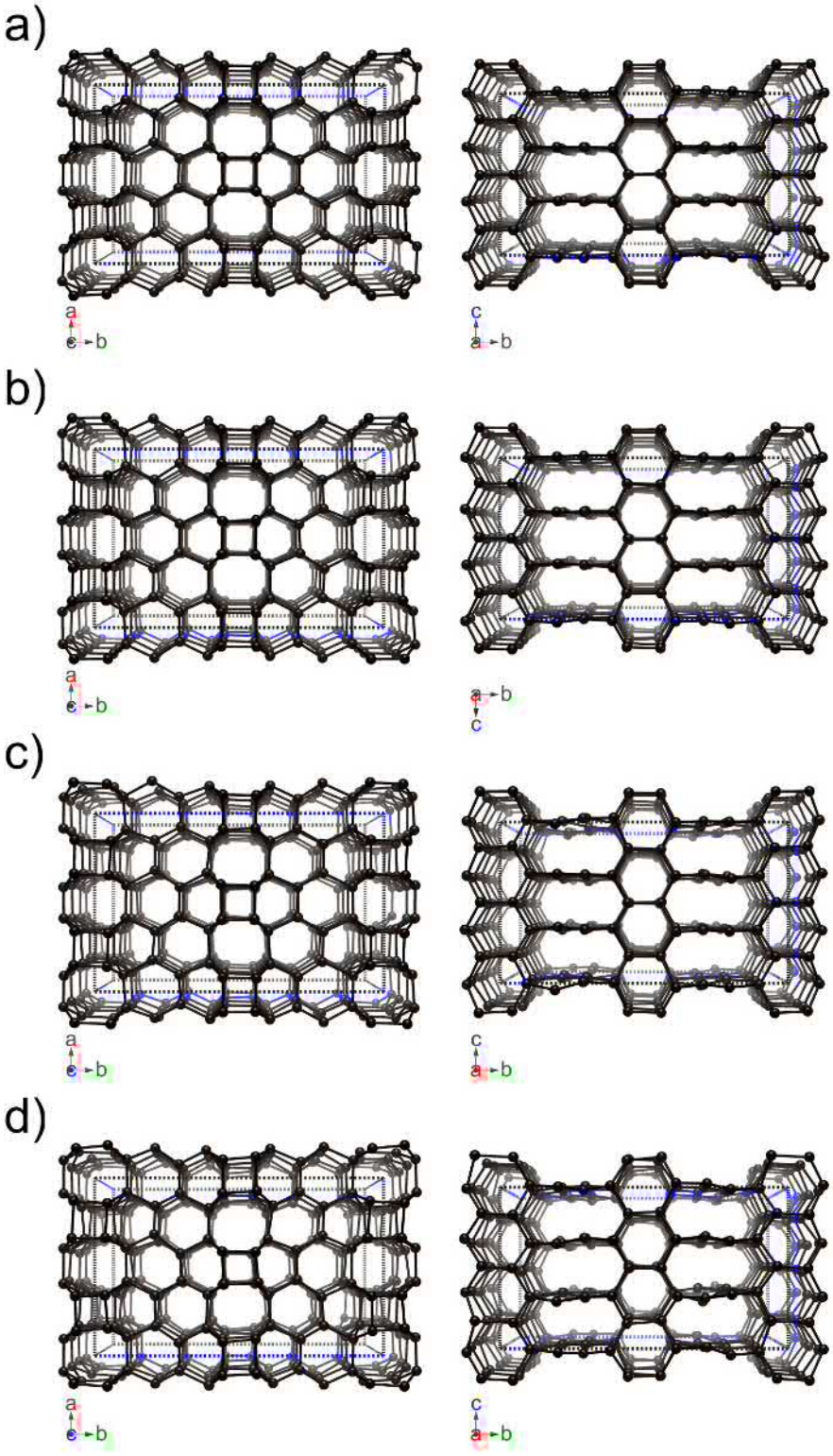

Figure S10: Top and side snapshots of the structures of DAC-carbon at: a) 100 K, b) 200 K, c) 300 K, and d) 400 K after 2.5 ps of MD simulation at 0 GPa.

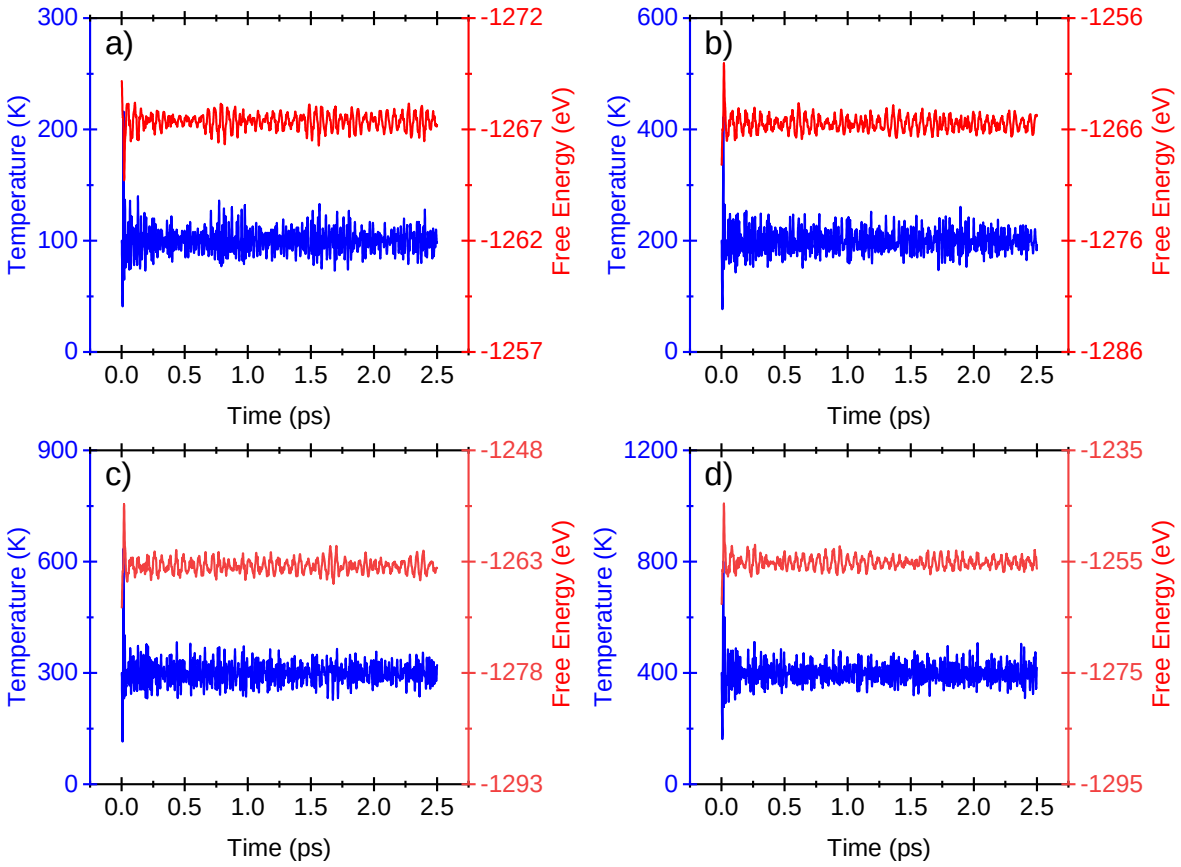

Figure S11: Temperature and energy profile for DAC-carbon at 20 GPa and: (a) 100 K, (b) 200 K, (c) 300 K, and (d) 400 K. All systems reached equilibrium within 0.2 ps.

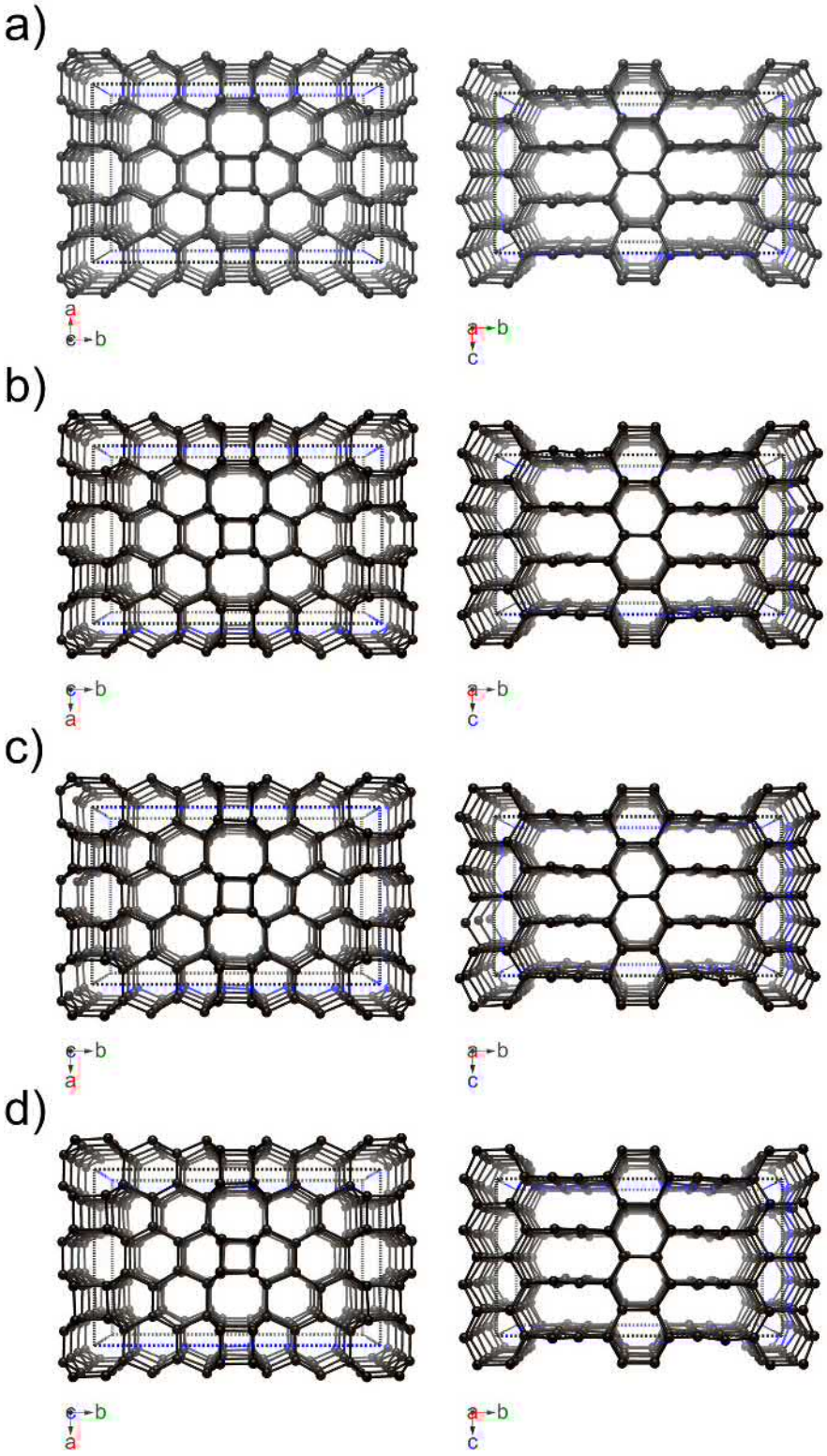

Figure S12: Top and side snapshots of the structures of DAC-carbon at: a) 100 K, b) 200 K, c) 300 K, and d) 400 K after 2.5 ps of MD simulation at 20 GPa.

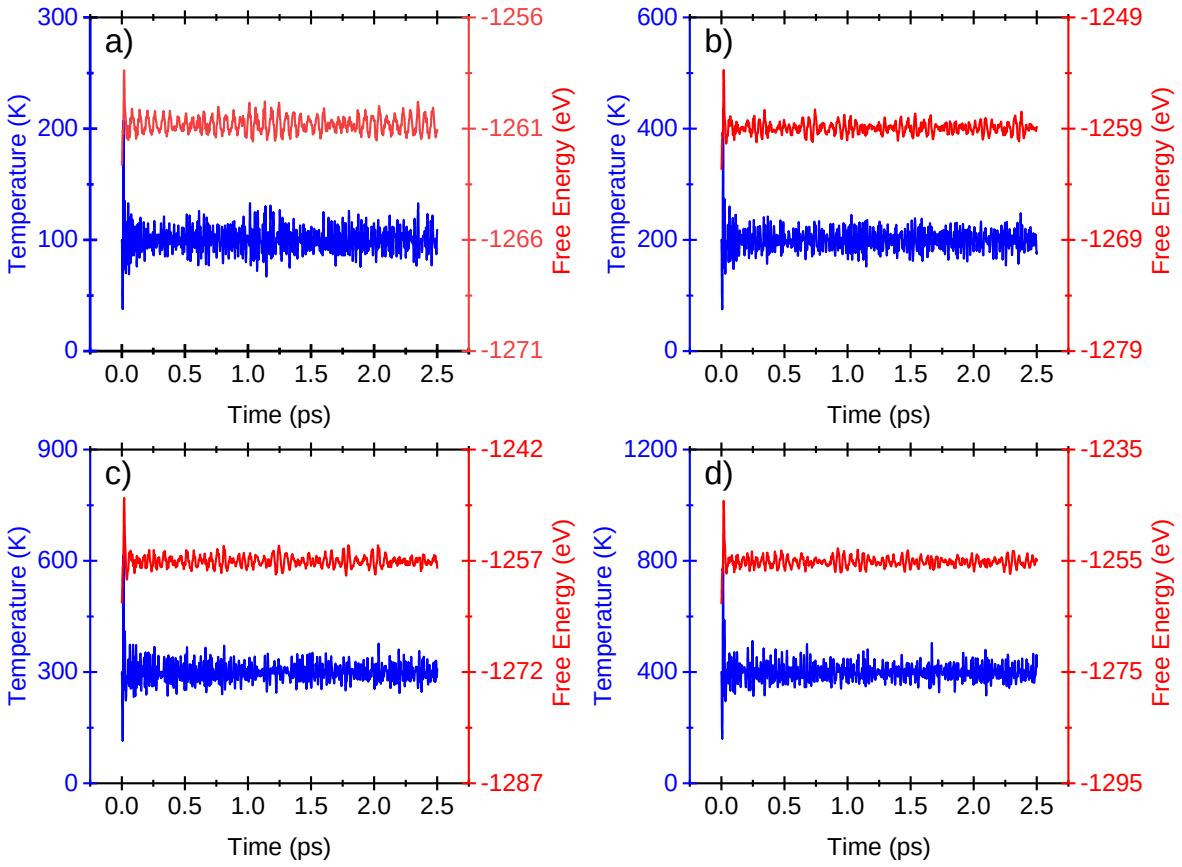

Figure S13: Temperature and energy profile for DAC-carbon at 40 GPa and: (a) 100 K, (b) 200 K, (c) 300 K, and (d) 400 K. All systems reached equilibrium within 0.2 ps.

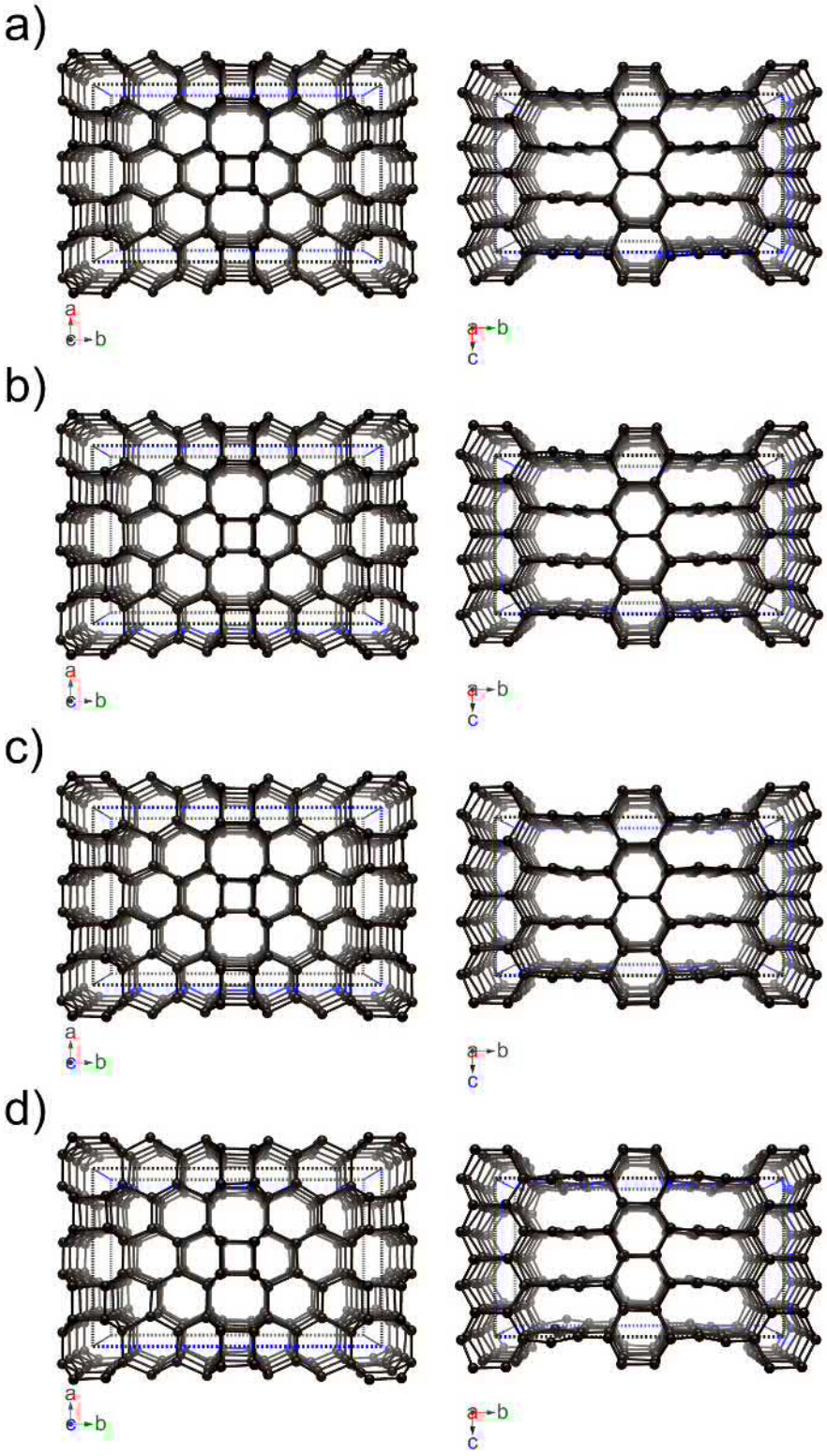

Figure S14: Top and side snapshots of the structures of DAC-carbon at: a) 100 K, b) 200 K, c) 300 K, and d) 400 K after 2.5 ps of MD simulation at 40 GPa.

S4.5 Approach to Synthesize DAC-Carbon

One way that DAC-carbon could be synthesized starts from armchair graphene nanoribbons (AGNRs), which have been studied intensely for their unique size and geometry-dependent properties.[40,41] GNRs were first predicted theoretically in 1996,[42] and since then researchers have found many ingenuous ways to synthesize structures with desired widths and edges (zigzag or armchair).[43,44]

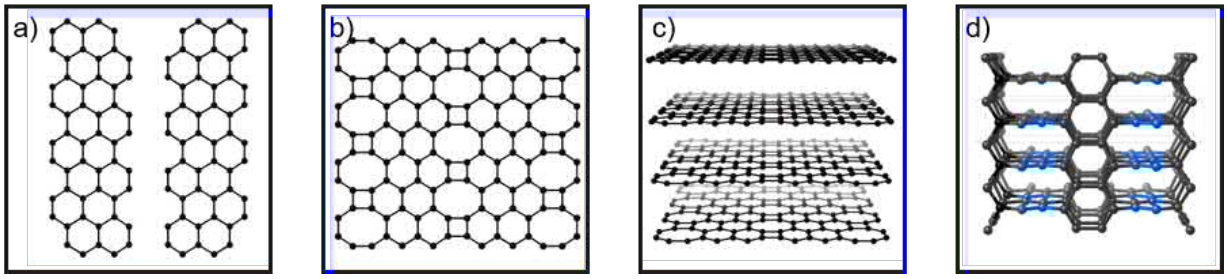

Figure S15: Proposed intermediates in the synthesis of DAC-Carbon. (a) 6-AGNRs are employed as precursors to (b) a 2D-DAC carbon sheet that contains 4,6 and 8 membered rings of sp^2 hybridized carbon atoms. (c) Multiple layers of 2D-DAC carbon are compressed to generate (d) crystalline DAC-carbon.

Figure S15 shows intermediate structures in our proposed synthesis of DAC-carbon. The synthesis begins with multiple 6-AGNRs (Figure S15a). Recently, a modular approach for the solution-phase synthesis of 6-AGNRs, based on polymerization of a single-aryl co-monomer (1,4-diborated benzene), has been reported.[45] Next, these nanoribbons would be used to synthesize a 2D network containing 4,6 and 8 membered carbon rings that we refer to as 2D-DAC carbon (Figure S15b). In fact, this network was recently proposed in a high-throughput study (65-3-12-r468-1).[46] It was found to be a semiconductor with a density of 0.361 carbon atoms/Å^2. We propose that this sheet could be made using on-surface interpolymer dehydrofluorination, which has recently been used to successfully synthesize a biphenylene network (called **jvh** in the Reticular Chemistry Structure Resource (RCSR) database[47]) with periodically arranged 4, 6 and 8 member rings of sp^2 hybridized carbon atoms starting from poly(2,5-difluoro-para-phenylene) (PFPP) on the Au(111) surface.[48] Compression of multiple layers of 2D DAC-carbon (Fig S15c) would yield 3D DAC-carbon (Fig S15d).

To study the precursors further, DFT calculations were carried out using the PBE functional[1] with Grimme's D3 dispersion correction (PBE-D3)[5] as implemented in VASP.[2] Phonon calculations revealed that a flat isolated sheet (with a vacuum spacing of 10 Å between layers) of 2D-DAC carbon is dynamically unstable, hinting that a non-planar geometry may be preferred instead. Indeed, *ab-initio* MD simulations with a single layer of 48 carbon atoms showed that the 2D network remains stable to at least 800 K, and it adopts a non-planar (wavy) structure as shown in Figure S16. This is not surprising given that non-hexagonal rings and defects in graphene analogues are known to induce such curvature creating "rippled" graphene-like layers.[49]

The (uniaxial) pressure at which crystalline DAC-carbon is estimated to become more stable than 2D DAC -arbon was determined by varying the interlayer distance and comparing the resulting energy with that of 3D DAC-carbon optimized at 0 GPa. Figure S17 shows that crystalline DAC-carbon becomes more stable than 2D sheets that are separated by less than 2.84 Å. This

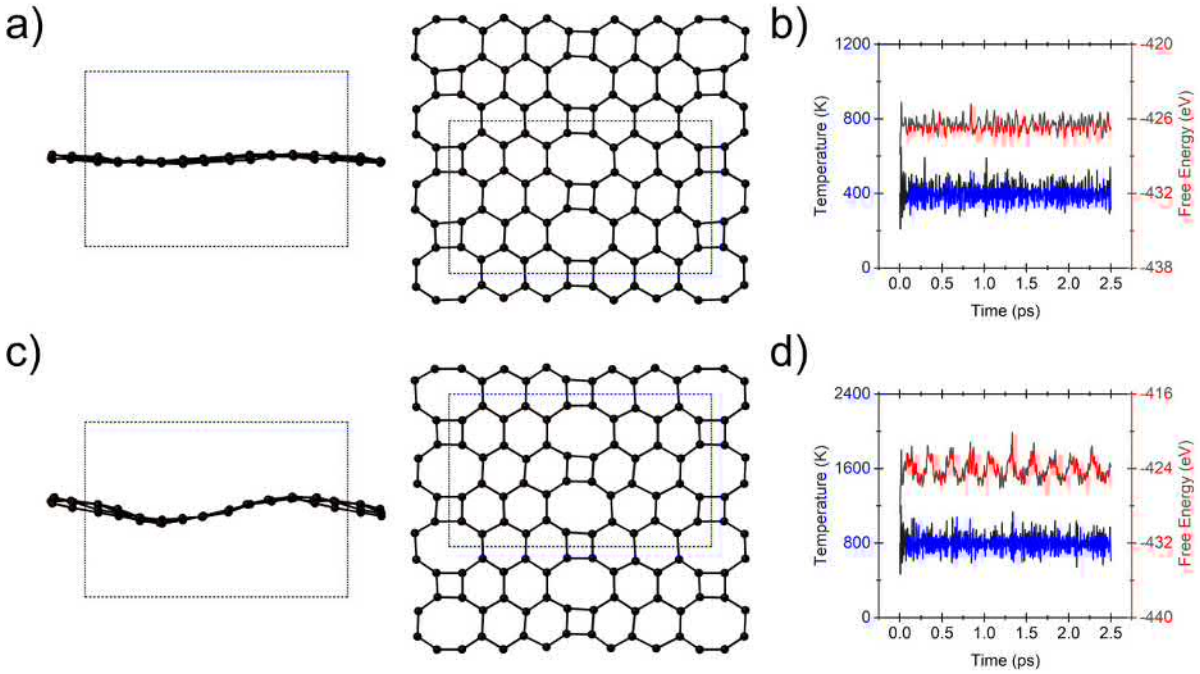

Figure S16: Top and side snapshots of the structures of 2D DAC-carbon at a) 400 K and c) 800 K after 2.5 ps of MD simulation at 0 GPa. Temperature and energy profile for 2D DAC-carbon at b) 400 K and d) 800 K and 0 GPa.

translates to a pressure of ∼20 GPa, as estimated using the method described in Section S4.3. Therefore, we postulate that compressing 2D DAC-carbon above 20 GPa would result in the formation of DAC-carbon, which would remain kinetically stable upon pressure release.

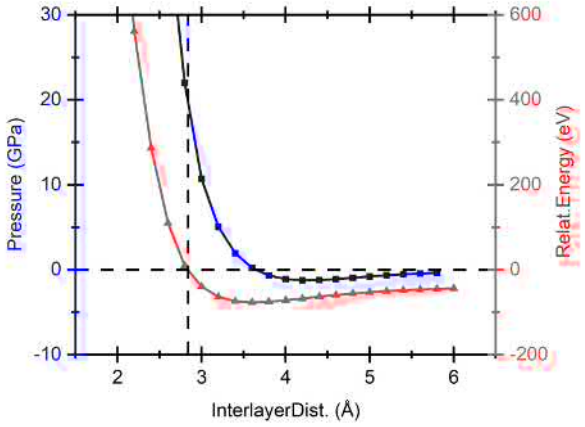

Figure S17: Energy of 2D DAC-carbon at the given interlayer distance relative to that of 3D DAC-carbon at zero pressure (red curve). Below 2.84 Å 3D-DAC carbon is energetically preferred. The pressure associated with the interlayer distance is estimated using the central difference method as described in Section S4.3 (blue curve).

S5 Optimized Structures for all Carbon Phases

Table S2: Calculated structural coordinates and enthalpies of metallic/semiconducting carbon allotropes (Figure S3).

Structure	$Cmmm$**-12b (DAC-carbon)**
Enthalpy (eV/atom)	**-8.860**
a, b, c (Å)	4.255 13.786 2.571
α, β, γ (Θ)	90.00 90.00 90.00
C (8q)	0.81606 0.10742 0.50000
C (8p)	0.31612 0.05677 0.00000
C (8q)	0.33492 0.20690 0.50000

Structure	$Cmmm$**-20**
Enthalpy (eV/atom)	**-8.865**
a, b, c (Å)	4.196 22.665 2.556
α, β, γ (Θ)	90.00 90.00 90.00
C (8q)	0.81431 0.18509 0.50000
C (8p)	0.68406 0.03453 0.00000
C (8p)	0.68638 0.21824 0.00000
C (8q)	0.66225 0.12546 0.50000
C (8q)	0.81615 0.06569 0.50000

Structure	$C2/m$**-16b**
Enthalpy (eV/atom)	**-8.906**
a, b, c (Å)	12.981 2.550 6.489
α, β, γ (Θ)	90.00 117.44 90.00
C (4i)	0.41914 0.00000 0.51582
C (4i)	0.77464 0.00000 0.07450
C (4i)	-0.09281 0.00000 0.16604
C (4i)	-0.05703 0.00000 -0.02639
C (4i)	0.16687 0.00000 0.26566
C (4i)	0.85342 0.00000 0.51717
C (4i)	0.74001 0.00000 0.27991
C (4i)	0.54897 0.00000 0.68724

Structure	$P1$**-16a**
Enthalpy (eV/atom)	**-8.814**
a, b, c (Å)	2.551 4.467 8.853
α, β, γ (Θ)	76.84 86.74 76.12
C (1a)	0.20783 0.73677 0.69091
C (1a)	0.75282 0.57996 0.64437
C (1a)	0.84600 0.06539 0.34396
C (1a)	0.70139 0.59586 -0.03532
C (1a)	0.86361 0.22277 0.00250
C (1a)	0.63089 0.55130 0.46785
C (1a)	0.06728 0.69112 0.37493
C (1a)	-0.01570 0.25359 0.71759
C (1a)	0.15840 0.73982 0.87205
C (1a)	0.70787 0.18309 0.49533
C (1a)	0.18117 0.07497 0.59840
C (1a)	-0.01264 0.09162 0.86168
C (1a)	0.40851 0.08823 0.09640
C (1a)	0.60445 0.71019 0.12342
C (1a)	0.31149 0.19889 0.25054
C (1a)	0.15237 0.57707 0.21780

Structure	$P1$**-16b**
Enthalpy (eV/atom)	**-8.810**
a, b, c (Å)	3.344 3.409 8.922
α, β, γ (Θ)	89.32 79.47 84.72
C (1a)	0.12670 0.00489 0.81290
C (1a)	0.38741 0.51637 0.61533
C (1a)	0.23215 0.82997 -0.03951
C (1a)	-0.02548 -0.01855 0.11070
C (1a)	-0.05643 0.82853 0.45048
C (1a)	0.19392 0.25644 0.20538
C (1a)	0.71628 0.82731 0.61625
C (1a)	0.78449 0.34493 0.81288
C (1a)	0.83932 0.61327 0.20099
C (1a)	0.26146 0.11524 0.36725
C (1a)	0.00188 0.67351 0.71802
C (1a)	0.50628 0.17339 0.70848
C (1a)	0.61977 0.75803 0.35721
C (1a)	0.61087 0.34138 0.11063
C (1a)	0.52950 0.51830 -0.03962
C (1a)	0.30912 0.49408 0.44962

Structure	$P\bar{1}$**-16b**
Enthalpy (eV/atom)	**-8.833**
a, b, c (Å)	2.536 4.354 8.646
α, β, γ (Θ)	96.82 93.23 92.23
C (2i)	0.23355 -0.07106 0.45637
C (2i)	0.27821 -0.02317 0.27781
C (2i)	0.83039 0.48722 0.27345
C (2i)	0.26010 0.59124 0.02895
C (2i)	0.69583 0.36475 0.79261
C (2i)	0.21718 0.86487 0.77958
C (2i)	0.02258 0.58583 0.44229
C (2i)	0.75357 0.09028 0.03214

Structure	$P\bar{1}$**-16c**
Enthalpy (eV/atom)	**-8.851**
a, b, c (Å)	2.544 4.367 8.541
α, β, γ (Θ)	87.63 85.00 87.74
C (2i)	0.05165 -0.09557 0.44196
C (2i)	0.38858 0.48646 0.27669
C (2i)	0.74502 0.43590 0.54381
C (2i)	0.49932 0.17012 -0.02663
C (2i)	0.01954 0.66776 -0.03396
C (2i)	-0.07949 0.31881 0.21961
C (2i)	0.05521 0.02528 0.72881
C (2i)	0.45209 0.81522 0.20510

Structure	$P\bar{1}$**-16e**
Enthalpy (eV/atom)	**-8.834**
a, b, c (Å)	2.538 4.353 8.575
α, β, γ (Θ)	86.81 86.90 87.71
C (2i)	0.02089 0.39438 0.05765
C (2i)	0.27277 -0.05010 0.22342
C (2i)	0.76456 -0.05521 -0.04416
C (2i)	0.74135 0.41285 0.53135
C (2i)	0.24883 -0.08612 0.52985
C (2i)	0.77368 0.10413 0.29027
C (2i)	0.17696 0.56200 0.77489
C (2i)	0.29850 0.60621 0.28131

Table S3: Calculated coordinates and enthalpies of carbon allotropes obtained from following the soft modes in DAC-carbon (see main text).

Structure	$Cmcm$ (following Z point)
a, b, c (Å)	13.884 4.279 4.829
α, β, γ (Θ)	90.00 90.00 90.00
C (16h)	0.39299 0.31673 -0.00448
C (8g)	-0.05434 0.31359 0.25000
C (8g)	0.55860 0.18253 0.25000
C (16h)	0.79289 0.33499 0.06174

Structure	$Ibam$ (following T point)
a, b, c (Å)	4.279 13.850 4.831
α, β, γ (Θ)	90.00 90.00 90.00
C (16k)	0.31672 0.10692 0.24460
C (8j)	0.31111 0.55288 0.00000
C (8j)	0.68034 0.55969 0.00000
C (16k)	0.83522 0.20713 0.31293

References

[1] J. P. Perdew, K. Burke, M. Ernzerhof, *Phys. Rev. Lett.* **1996**, *77*, 3865.

[2] G. Kresse, J. Hafner, *Phys. Rev. B.* **1993**, *47*, 558.

[3] P. E. Blochl, *Phys. Rev. B* **1994**, *50*, 17953.

[4] H. J. Monkhorst, J. D. Pack, *Phys. Rev. B* **1976**, *13*, 5188.

[5] S. Grimme, J. Antony, S. Ehrlich, H. Krieg, *J. Chem. Phys.* **2010**, *132*, 154104.

[6] A. V. Krukau, O. A. Vydrov, A. F. Izmaylov, G. E. Scuseria, *J. Chem. Phys.* **2006**, *125*, 224106.

[7] R. Dronskowski, P. E. Bloechl, *J. Phys. Chem.* **1993**, *97*, 8617–8624.

[8] S. Maintz, V. L. Deringer, A. L. Tchougréeff, R. Dronskowski, *LOBSTER: A tool to extract chemical bonding from plane-wave based DFT*, **2016**.

[9] D. M. Teter, *Mrs Bull.* **1998**, *23*, 22–27.

[10] O. Isayev, C. Oses, C. Toher, E. Gossett, S. Curtarolo, A. Tropsha, *Nat. Commun.* **2017**, *8*, 15679.

[11] P. Avery, X. Wang, C. Oses, E. Gossett, D. M. Proserpio, C. Toher, S. Curtarolo, E. Zurek, *npj Comp. Mater.* **2019**, *5*, 1–11.

[12] A. Togo, I. Tanaka, *Scr. Mater.* **2015**, *108*, 1–5.

[13] S. Nosé, *J. Chem. Phys.* **1984**, *81*, 511–519.

[14] W. G. Hoover, *Phys. Rev. A* **1985**, *31*, 1695.

[15] P. Giannozzi, O. Andreussi, T. Brumme, O. Bunau, M. B. Nardelli, M. Calandra, R. Car, C. Cavazzoni, D. Ceresoli, M. Cococcioni, *J. Phys. Cond. Mat.* **2017**, *29*, 465901.

[16] A. Dal Corso, *Comput. Mater. Sci.* **2014**, *95*, 337–350.

[17] P. B. Allen, R. C. Dynes, *Phys. Rev. B* **1975**, *12*, 905.

[18] R. Hoffmann, T. Hughbanks, M. Kertesz, P. H. Bird, *J. Am. Chem. Soc.* **1983**, *105*, 4831–4832.

[19] A. Y. Liu, M. L. Cohen, *Phys. Rev. B* **1992**, *45*, 4579.

[20] M. A. Tamor, K. Hass, *J. Mat. Res.* **1990**, *5*, 2273–2276.

[21] M. J. Bucknum, R. Hoffmann, *J. Am. Chem. Soc.* **1994**, *116*, 11456–11464.

[22] M. Itoh, M. Kotani, H. Naito, T. Sunada, Y. Kawazoe, T. Adschiri, *Phys. Rev. Lett.* **2009**, *102*, 055703.

[23] Y. Cheng, R. Melnik, Y. Kawazoe, B. Wen, *Cryst. Growth Des.* **2016**, *16*, 1360–1365.

[24] C.-Y. Niu, X.-Q. Wang, J.-T. Wang, *J. Chem. Phys.* **2014**, *140*, 054514.

[25] X. Zhu, H. Yan, X. Wang, M. Zhang, Q. Wei, *Results Phys.* **2019**, *15*, 102738.

[26] M. Hu, X. Dong, Y. Wu, L. Liu, Z. Zhao, X.-F. Zhou, T. A. Strobel, G. Gao, Y. Tian, J. He, *Dalton Trans.* **2018**, *47*, 6233–6239.

[27] A. Kuc, G. Seifert, *Phys. Rev. B* **2006**, *74*, 214104.

[28] M. Hu, Z. Zhao, F. Tian, A. R. Oganov, Q. Wang, M. Xiong, C. Fan, B. Wen, J. He, D. Yu *et al.*, *Sci. Rep.* **2013**, *3*, 1–7.

[29] C. Zhao, C. Niu, Z. Qin, X. Y. Ren, J. Wang, J. Cho, Y. Jia, *Sci. Rep.* **2016**, *6*, 21879.

[30] X. Wu, X. Shi, M. Yao, S. Liu, X. Yang, L. Zhu, T. Cui, B. Liu, *Carbon* **2017**, *123*, 311–317.

[31] F. J. Ribeiro, P. Tangney, S. G. Louie, M. L. Cohen, *Phys. Rev. B* **2005**, *72*, 214109.

[32] M. Hu, M. Ma, Z. Zhao, D. Yu, J. He, *AIP Adv.* **2016**, *6*, 055020.

[33] M. Hu, X. Dong, B. Yang, B. Xu, D. Yu, J. He, *Phys. Chem. Chem. Phys.* **2015**, *17*, 13028–13033.

[34] Y. Liu, X. Jiang, J. Fu, J. Zhao, *Carbon* **2018**, *126*, 601–610.

[35] L. Liu, M. Hu, Z. Zhao, Y. Pan, H. Dong, *Carbon* **2020**, *158*, 546–552.

[36] W. Zhang, C. Chai, Q. Fan, Y. Song, Y. Yang, *Diam. Relat. Mater.* **2020**, *109*, 108063.

[37] W. Zhang, C. Chai, Q. Fan, Y. Song, Y. Yang, *New J. Chem.* **2020**, *44*, 19789–19795.

[38] W. Zhang, C. Chai, Y. Song, Q. Fan, Y. Yang, *Diam. Relat. Mater.* **2021**, *120*, 108706.

[39] J. Chen, P. Ying, Y. Gao, X. Wei, B. Li, Q. Huan, K. Luo, *J. Mater. Sci.* **2021**, *56*, 17665–17673.

[40] R. K. Houtsma, J. de la Rie, M. Stöhr, *Chem. Soc. Rev.* **2021**, *50*, 6541–6568.

[41] H. Wang, H. S. Wang, C. Ma, L. Chen, C. Jiang, C. Chen, X. Xie, A.-P. Li, X. Wang, *Nat. Rev. Phys.* **2021**, *3*, 791–802.

[42] M. Fujita, K. Wakabayashi, K. Nakada, K. Kusakabe, *J. Phys. Soc. Jpn.* **1996**, *65*, 1920–1923.

[43] A. Kimouche, M. M. Ervasti, R. Drost, S. Halonen, A. Harju, P. M. Joensuu, J. Sainio, P. Liljeroth, *Nat. Comm.* **2015**, *6*, 10177(1–6).

[44] Z. Chen, A. Narita, K. Müllen, *Adv. Mater.* **2020**, *32*, 2001893.

[45] G. Li, K.-Y. Yoon, X. Zhong, J. Wang, R. Zhang, J. R. Guest, J. Wen, X.-Y. Zhu, G. Dong, *Nat. Comm.* **2018**, *9*, 1–9.

[46] X. Shi, S. Li, J. Li, T. Ouyang, C. Zhang, C. Tang, C. He, J. Zhong, *J. Phys. Chem. Lett.* **2021**, *12*, 11511–11519.

[47] *jvh topology in the Reticular Chemistry Structure Resource database*, `http://rcsr.net/layers/jvh`, Accessed: 2022-06-05.

[48] Q. Fan, L. Yan, M. W. Tripp, O. Krejčí, S. Dimosthenous, S. R. Kachel, M. Chen, A. S. Foster, U. Koert, P. Liljeroth *et al.*, *Science* **2021**, *372*, 852–856.

[49] F. L. Thiemann, P. Rowe, A. Zen, E. A. Muller, A. Michaelides, *Nano Lett.* **2021**, *21*, 8143–8150.